Nonlin. Processes Geophys. Discuss., doi:10.5194/npg-2017-8, 2017
Manuscript under review for journal Nonlin. Processes Geophys.
Discussion started: 16 February 2017

Nonlinear Processes in Geophysics
Discussions
Open Access
EGU

Insights on the three-dimensional Lagrangian geometry of the Antarctic Polar Vortex

Jezabel Curbelo[1,2], Víctor J. García-Garrido[1], Carlos R. Mechoso[3], Ana M. Mancho[1], Stephen Wiggins[4], and Coumba Niang[1,5]

[1]Instituto de Ciencias Matemáticas, CSIC-UAM-UC3M-UCM. C/ Nicolás Cabrera 15, Campus de Cantoblanco UAM, 28049 Madrid, Spain.
[2]Departamento de Matemáticas, Facultad de Ciencias, Universidad Autonóma de Madrid, 28049 Madrid, Spain.
[3]Department of Atmospheric and Oceanic Sciences, University of California at Los Angeles, Los Angeles, California.
[4]School of Mathematics, University of Bristol. Bristol BS8 1TW, UK.
[5]Laboratoire de Physique de l'Atmosphere et de l'Ocean Simeon Fongang, Ecole Superieure Polytechnique, Universite Cheikh Anta Diop, 5085, Dakar-Fann, Senegal.

Abstract. The present paper introduces an algorithm for the visualization, analysis and verification of transport and mixing processes in three-dimensional atmospheric flows. This algorithm is based on the methodology of Lagrangian descriptors (LDs), a technique from Dynamical Systems Theory. The algorithm is applied to reanalysis data in order to illustrate the evolution of the flow above Antarctica during a period of rapid changes in the southern spring of 1979. The evolution of Lagrangian coherent structures is discussed and connections with the stratosphere is examined. The results suggest that the cyclonic stratospheric polar vortex during late winter appears to extend down to the troposphere. The results are also indicative of features related to invariant manifolds that can act as deep vertical barriers to transport between vortices.

1 Introduction

Over the past several decades the mathematical theory of dynamical systems has provided a fruitful framework to describe the transport and mixing proceses that take place in fluids and to understand the underlying flow structures associated with these phenomena. The seminal paper by Aref (1984) on chaotic advection sparked interest in this perspective, which is inspired by the work of Poincaré. For the understanding of particle dynamics, Poincaré sought a geometrical approach that was based on geometrical structures and their role in organizing all trajectories into regions corresponding to qualitatively different dynamical fates. These structures have been referred to as Lagrangian Coherent Structures (LCS) in the fluid mechanics community (Haller and Yuan, 2000; Shadden *et al.*, 2005).

Many studies of LCS in the atmosphere and in the ocean have been performed in a two-dimensional (2D) scenario. This is because in an appropriate range of space and time scales a Lagrangian property of the particles is approximately unchanged in time. Hence, the flow can be assumed to occur on surfaces on which that property is constant. For instance, stratospheric flows in the time scale of stratospheric sudden warmings (∼10 days) are, to a first approximation, adiabatic and frictionless, and thus fluid particles and their trajectories are constrained to remain on surfaces of constant specific potential temperature (isentropic surfaces). Bowman (1993) and Koh and Legras (2002) have examined transport processes across the Antarctic

Nonlin. Processes Geophys. Discuss., doi:10.5194/npg-2017-8, 2017
Manuscript under review for journal Nonlin. Processes Geophys.
Discussion started: 16 February 2017

Nonlinear Processes in Geophysics Discussions
Open Access
EGU

stratospheric polar vortex (SPV) on isentropic surfaces, which are quasi-horizontal in the atmosphere. Also, for oceanic flows it is often assumed that fluid parcels remain on surfaces of constant density (isopycnals), which are quasi-horizontal. Mancho *et al.* (2006); d'Ovidio *et al.* (2009); Branicki *et al.* (2011) followed the isopycnal approach for oceanic applications in the Mediterranean Sea, Mendoza *et al.* (2014) for the Gulf of Mexico and Garcia-Garrido *et al.* (2015, 2016) for other ocean areas.

Geophysical flows, however, are not 2D. The study of transport processes in 3D flows brings into the discussion issues about the three-dimensional (3D) visualization of Lagrangian structures (see e.g. Wiggins (2010)). In idealized 3D time-dependent flows Poincaré sections have been used to recognize significant Lagrangian structures (Cartwright *et al.*, 1996; Pouransari *et al.*, 2010; Moharana *et al.*, 2013; Rypina *et al.*, 2015). Invariant manifolds acting as transport barriers in 3D flows may have the structure of convoluted 2D surfaces embedded in a volume (Branicki and Wiggins, 2009). In oceanic contexts these surfaces have been identified by stitching together 2D Lagrangian structures at different layers (Branicki and Kirwan Jr., 2010) or connecting ridges computed from Finite Size Lyapunov exponent fields (Bettencourt *et al.*, 2014). In the field of atmospheric sciences, these structures have similarly been obtained by connecting ridges computed from Finite Time Lyapunov Exponents (FTLE) (Rutherford and Dangelmayr, 2010; du Toit and Marsden, 2010; Lekien and Ross, 2010). More recently, also in atmospheric contexts, 3D Lagrangian information has been extracted by means of 2D slices of the full 3D FTLE field computed from 3D trajectories (Rutherford *et al.*, 2012).

The present paper introduces an algorithm for the visualization, analysis and validation of transport and mixing processes in 3D atmospheric flows. The methodology is based on the Lagrangian descriptor known as the function M (Madrid and Mancho, 2009; Mendoza and Mancho, 2010; Mancho *et al.*, 2013), computed in 3D. So far, the function M has been used in 2D settings to gain insight into key dynamical and transport processes in the stratosphere (de la Cámara *et al.*, 2012, 2013; Smith and McDonald, 2014; Guha *et al.*, 2016; Manney and Lawrence, 2016; García-Garrido *et al.*, 2017). More recently, (Mancho *et al.*, 2013; Lopesino *et al.*, 2017) have applied the function M to the visualization of structures in idealized 3D flows. Rempel *et al.* (2013) have applied the function M to visualize coherent structures in full 3D direct numerical simulations of the compressible magnetohydrodynamic equations. The function M has the advantage of highlighting simultaneously invariant manifolds by means of singular features and also tori-like coherent structures (see Mendoza and Mancho (2010); de la Cámara *et al.* (2012); Rempel *et al.* (2013); Lopesino *et al.* (2017)). In here we apply M to produce a full 3D description from 3D flows above Antarctica during a period in the spring of 1979 when there were rapid changes in the stratosphere (Yamazaki and Mechoso, 1985). In this region, the period selected for analysis comprises an interval when the winter circulation, which is characterized by a strong circumpolar westerly (cyclonic) flow known as the Stratospheric Polar Vortex (SPV), breaks down as the final warming to summer condition develops. Although final warmings in the southern hemisphere are broadly similar each year (Mechoso *et al.*, 1988), can be punctuated by periods of rapid changes. During the final warming of 1979, the transition from the winter to the summer circulation accelerated during mid-October, a period when perturbing waves were very active and the vertical energy flux from the troposphere intensified (Yamazaki and Mechoso, 1985). Our aim is to describe and visualize these phenomena from a full 3D perspective using reanalysis data. To our knowledge, this is the first time that the potential of M to achieve this goal is explored.

Nonlin. Processes Geophys. Discuss., doi:10.5194/npg-2017-8, 2017
Manuscript under review for journal Nonlin. Processes Geophys.
Discussion started: 16 February 2017

The article is organized as follows. Section 2 describes the dataset used for the study of the Antarctic final warming of 1979 and the post-processing needed for the Lagrangian analysis. Section 3 describes the calculation of M in 3D and details the computational procedures and issues involved in this task. Section 4 discusses the results and findings of M on the 3D Lagrangian structure of the polar vortex on August and mid-October 1979. Finally, section 5 includes a discussion and presents our conclusions.

2 Dataset and Post-processing

2.1 ERA-Interim Reanalysis Data

We use the ERA-Interim Reanalysis dataset produced European Centre for Medium-Range Weather Forecasts (ECMWF;Simmons *et al.* (2007)). The usefulness of this dataset for the Lagrangian study of atmospheric flows from the dynamical systems perspective is assured by the results of several previous studies. For instance, de la Cámara *et al.* (2013) applied Lagrangian Descriptors (LDs) to study the structure of the southern polar vortex during the 2005 southern spring and compared the LCS obtained with the trajectories of superpressure balloons released from Antarctica by the VORCORE project (Rabier *et al.*, 2010). ERA-Interim covers the period from 1979 to the present day (Dee *et al.*, 2011) and it can be downloaded from http://apps.ecmwf.int/datasets/data/interim-full-daily/levtype=sfc/.

From the ERA-Interim dataset we use the wind velocity components, potential vorticity, surface pressure and also geopotential field. These physical variables are available four times daily (00:00 06:00 12:00 18:00 UTC) with a horizontal resolution of $0.75° \times 0.75°$ in longitude and latitude. We take the velocity fields at the sigma levels of the model component of the reanalysis system (60 levels in the vertical from 1000 to 0.1 hPa). Moreover, we take potential vorticity at 15 levels of potential temperature (265, 275, 285, 300, 315, 330, 350, 370, 395, 430, 475, 530, 600, 700, 850), and geopotential field at hPa pressure levels (1, 2, 3, 5, 7, 10, 20, 30, 50, 70, 100 to 250 by 25, 300 to 750 by 50, 775 to 1000 by 25). For the calculation of parcel trajectories, as needed to compute the function M, the wind fields are transformed from sigma to geometric height (80 levels that range from 0 m to 47600 m with a step of 600 m).

2.2 Data post-processing

Our goal is to compute particle trajectories on spatial coordinates, and for this reason we need to transform the wind fields from the model levels (used in the ERA-Interim Reanalysis) to height (in meters). For the post-processing of the dataset we use the Climate Data Operator (CDO) software (available at https://code.zmaw.de/projects/cdo). The input provided to the CDO consists of the three velocity components in sigma levels, and of surface pressure, which is available every six hours on a global grid of $0.75° \times 0.75°$. The data is downloaded from ERA-Interim in `.grib` format and on a monthly basis and is stored daily in separate files in order to avoid handling very large data files when computing particle trajectories that require interpolation.

To transform the data from hybrid sigma (model) levels to height using CDO, first one concatenates each wind component with the surface pressure using the CDO command `merge` and later one needs to convert the data files from `.grib` to `.nc`

Nonlin. Processes Geophys. Discuss., doi:10.5194/npg-2017-8, 2017
Manuscript under review for journal Nonlin. Processes Geophys.
Discussion started: 16 February 2017

Nonlinear Processes in Geophysics Discussions
Open Access
EGU

format. This is done with the command `copy`, setting as arguments `-t ecmwf` to indicate that the data is from ERA-Interim and `-f nc` to specify that the output complies with NetCDF. Next, we apply the CDO command `ml2hlx` to the NetCDF files, which converts data at the sigma levels of ERA-Interim to the height levels that we select for our analysis and extrapolate the missing data. The vertical spatial interpolation is performed over 80 height levels that range from 0 m to 47600 m with a step of 600 m. Each wind data variable is stored in separate files by day; the commands `selvar` and `selday` are used for this process.

3 The Dynamical Systems Approach to the Analysis of Lagrangian Structures

The theory of dynamical systems provides an ideal framework for studying nonlinear transport and mixing processes in the atmosphere. The geometrical structures that vertebrate the Lagrangian skeleton act as material barriers that fluid particles cannot cross. A key element on the dynamical description is the distinction between hyperbolic and elliptic regions. Hyperbolic regions are defined by rapid fluid contracting and expanding rates along directions that are respectively associated to the stable and unstable manifolds. In 2D flows, these manifolds are curves while in 3D settings other possibilities arise in which manifolds are complex and convoluted 2D surfaces embedded in the 3D space. This makes the array of possible spatial configurations richer and their visualization much more complex. A discussion on the notion of elliptic regions is given for instance in (Mancho *et al.*, 2013). Heuristically for us in this article, this notion is related to fluid regions trapping fluid parcels in their interior and isolating them from the surrounding fluid as for instance is the case of the circulating strong jet forming the SPV.

The diagnostic that we will use to build the Lagrangian skeleton of the atmosphere is the function M, which is defined in the following way:

$$M(\mathbf{x}_0, t_0, \tau) = \int_{t_0-\tau}^{t_0+\tau} \|\mathbf{v}(\mathbf{x}(t;\mathbf{x}_0),t)\|\, dt\,, \tag{1}$$

where $\mathbf{v}(\mathbf{x},t)$ is the velocity field and $\|\cdot\|$ denotes the Euclidean norm. At a given time t_0, M corresponds to the length of the trajectory traced by a fluid parcel starting at $\mathbf{x}_0 = \mathbf{x}(t_0)$ as it evolves forwards and backwards in time for a time interval τ. As τ increases a richer Lagrangian history is incorporated into M, and a more complex and detailed dynamical description is obtained. The sharp changes that occur in narrow gaps in the scalar field provided by M, which we will refer to as singular features, highlight the stable and unstable manifolds and, at their crossings, hyperbolic trajectories (see for example Fig. 1). This tool has also the capability of revealing the vortices present in the fluid. Recently, Lopesino *et al.* (2017) have established a rigorous mathematical foundation (at specific examples) for specific LDs in continuous time dynamical systems.

If we assume that air parcels are passively advected by the flow, the dynamical system that governs the atmospheric flow is given by:

$$\dot{\mathbf{x}} = \mathbf{v}\left(\mathbf{x}\left(t\right),t\right) \;\;,\;\; \mathbf{x}\left(t_0\right) = \mathbf{x}_0\,, \tag{2}$$

where $\mathbf{x}\left(t;\mathbf{x}_0\right)$ represents the trajectory of an air parcel that at time t_0 is at position $\mathbf{x}_0$, and $\mathbf{v}$ is th velocity field.

Nonlin. Processes Geophys. Discuss., doi:10.5194/npg-2017-8, 2017
Manuscript under review for journal Nonlin. Processes Geophys.
Discussion started: 16 February 2017

Nonlinear Processes in Geophysics
Discussions
Open Access
EGU

The computation of M requires the integration of particle trajectories by means of numerically integrating (2). In geographic coordinates Eq. (2) can be written as:

$$\begin{cases} \dfrac{d\lambda}{dt} = \dfrac{u(\lambda,\phi,h,t)}{(R+h)\cos\phi} \\ \dfrac{d\phi}{dt} = \dfrac{v(\lambda,\phi,h,t)}{R+h} \\ \dfrac{dh}{dt} = w(\lambda,\phi,h,t) \end{cases} , \tag{3}$$

where u, v, and w are the zonal, meridional, and vertical velocity components, respectively, λ is longitude, ϕ is latitude, h is elevation (height) above the Earth's surface and $R = 6371$ km is the mean Earth radius. Observe that in these spherical coordinates there is a singularity at the poles. To avoid this issue, we will calculate trajectories using a cartesian coordinate system, the equations for the trajectories in this system are:

$$\begin{cases} \dfrac{dx}{dt} = v_x(\lambda,\phi,h,t) \\ \dfrac{dy}{dt} = v_y(\lambda,\phi,h,t) \\ \dfrac{dz}{dt} = v_z(\lambda,\phi,h,t) \end{cases} , \tag{4}$$

in which the velocity components are given by:

$$\begin{cases} v_x = w\cos\lambda\cos\phi - u\sin\lambda - v\cos\lambda\sin\phi \\ v_y = w\sin\lambda\cos\phi + u\cos\lambda - v\sin\lambda\sin\phi \\ v_z = w\sin\phi + v\cos\phi \end{cases} . \tag{5}$$

To integrate the system (4) the data interpolation of the fields v_x, v_y, v_z is carried out by interpolating u, v, w in spherical coordinates, since the post-processed data files from ERA-Interim are expressed in this way. In order to do so, we have used the `griddedInterpolant` function provided by the MATLAB© software, which generates an object that can be saved into memory and evaluated at any point of interest in the trajectory at a later time. This allows us substantial saving in computational time at every integration step. Moreover, when applying this function to interpolate the dataset, we specify that a cubic interpolation is used in space and also in time. The dynamical system (4) is integrated using a Cash-Karp Runge-Kutta scheme (Press *et al.*, 1992) with a time step of 1 hour and we impose the boundary condition of $w = 0$ for the vertical velocity of air particles at the Earth's surface (i.e. $h = 0$). Important computational savings are also achieved by integrating simultaneously the whole meshgrid of initial conditions by using a matrix formulation. Additionally, the computational time is reduced by running the MATLAB© software with options requiring the use of multiple cores.

Nonlin. Processes Geophys. Discuss., doi:10.5194/npg-2017-8, 2017
Manuscript under review for journal Nonlin. Processes Geophys.
Discussion started: 16 February 2017

Nonlinear Processes in Geophysics
Discussions
Open Access
EGU

4 Results

4.1 Benchmark simulations

As indicated earlier, the trajectories of fluid particles in stratospheric flows at time scale of ~ 10 days remain, to a first approximation, on surfaces of constant specific potential temperature (isentropic surfaces) which are themselves quasi-horizontal. A first step to benchmark the methodology described in the previous sections is to compare the Lagrangian outputs obtained from the full 3D scenario at a constant height with those obtained from the 2D scenario for a potential temperature surface that is at approximately the same height. Figure 1a) shows the evaluation of the function M with $\tau = 5$ days for a 2D integration in the 850K isentropic surface. The figure highlights well defined structures (de la Cámara *et al.*, 2012). These consist of large circulating coherent vortex in yellow, representing high values of M that are related to particles exhibiting large displacements and blueish zones corresponding to calmer regions. Lobes eroding the outer part of the vortex are clearly identified by colored filaments. Also crossings of contours of M highlighting hyperbolic trajectories are noticed along longitudes 15^{o}W and 165 ^{o}E. The height level that corresponds to the 850K surface is approximately 31.3km. Figure 1b) shows the output of M at this constant height for a full 3D integration with $\tau = 5$. A very similar pattern is found, which supports the correctness of the results reflecting the small departures of fluid particles from the quasi-horizontal isentropic surface in the time scale of a few days.

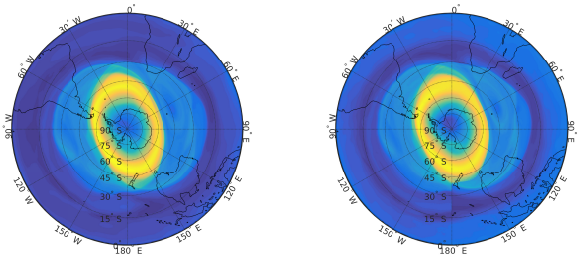

a) b)

Figure 1. M calculated on the 15th August at 1979 00:00:00 UTC with $\tau = 5$: a) using a 2D approach where particle trajectories are constrained to the 850K potential temperature level; b) using a 3D computation of trajectories and represented at a constant height level of $h = 31.3$ km (which corresponds approximately to the 850K isentropic surface).

Figure 2 shows further comparisons at different days in October 1979. The left hand column shows the geopotential height at 10mb. This field is related with the velocity streamfunction at the corresponding presure level (see García-Garrido *et al.* (2017)). The middle column shows the potential vorticity at the 850K equivalent temperature (isentropic) surface. In the right hand column we show outputs obtained from 3D calculations of the function M at the surface $z = 31.3$km. These results are further demonstration of the consistency of our algorithm.

Nonlin. Processes Geophys. Discuss., doi:10.5194/npg-2017-8, 2017
Manuscript under review for journal Nonlin. Processes Geophys.
Discussion started: 16 February 2017

Nonlinear Processes in Geophysics
Discussions
Open Access
EGU

4.2 3D Lagrangian structures over Antarctica

The strong and cyclonic SPV characteristic of the winter circulation above Antarctica is typically represented by cross sections such as those in Figs. 1 and 2. In this section we attempt to improve on this representation with figures that are more revealing of the full 3D description of the circulation. Figure 3 shows for a day in late winter 1979 (15th of August) the representation of M obtained for $\tau = 5$ for the vertical slice passing through longitudes 90^oW and 90^oE. An outstanding feature in this representation is the bright yellow color highlighting a coherent structure. This feature captures the SPV as a tubular structure with walls around 60^0S and an approximately vertical axis coinciding with that of the Earth and extending from the uppermost level of data down to between 15 and 20 km height, i.e. the transition between troposphere and stratosphere (tropopause). On the one hand, the greenish colors that extend equatorward between 15 and 20 km, both at the west and the east, capture the upper tropospheric subtropical westerly jets. Specifically at the west , the greenish colors extend downwards up to the equator (90^oW) suggesting that the structures involve the entire atmospheric layer. We can also clearly see evidence of the very different dynamical character of the troposphere and stratosphere. Whilst the former region is practically dominated by the SPV, the latter shows much more fine detail reflected by an intricate line pattern. This tangled pattern is the manifestation of crossings of stable and unstable manifolds, which are associated with strong and fast mixing processes at the lowest atmospheric levels.

The description of the vortex on the 15th August 1979 is supplemented by Fig. 4, which shows the function M computed for $\tau = 5$ along a vertical slice through latitude 60°S, where most of the SPV walls are. The intricate structures in the troposphere are also apparent in this figure. In addition, a wavy structure is clearly visible at the boundary between troposphere and stratosphere. In terms of a Fourier decomposition of M at constant height in Fig. 4, we can see the classical pattern of longer wavelengths dominating the field as height increases. At tropopause level, a wavenumber 4 component is clearly visible while at the upper part of the vortex a wavenumber 2 is evident. The vertical propagation of these features across the stratosphere from the 8th to the 21st of August of 1979 is clearly visible in the attached movie S1.

Figure 5 shows the rapid changes of the SPV that took place in October 1979 as the lower polar stratosphere warmed up strongly during the spring season (Yamazaki and Mechoso, 1985). The figure shows the function M computed for $\tau = 5$ along a vertical slice passing through latitude 60°S for several October dates. To help in the interpretation of Fig. 5, Fig. 6 displays horizontal sections of M on the 6th of October at different heights $z = 10$km, 21.2km, 31.3km and 40km. Figure 5 shows sharp contrasts with the winter conditions two months earlier visible in Figs. 3 and 4. The structure representing the cyclonic vortex tube flow is now approximately centered off the pole above the Antarctic Peninsula at lower levels in the stratosphere. The 60°S section in Fig. 5 a) intersects the cyclonic vortex four times mostly in the western hemisphere. Another deep, anticyclonic vortex appears in the eastern hemisphere above 25km. This is evident in Fig. 5 a), Fig. 6a) at $z = 31.3$km and $z = 40$km and in Fig. 6b). Mechoso and Hartmann (1982) suggest that the preferred geographical location (ridge south of Australia) for development of the anticyclonic vortex indicate that the stratospheric circulation is governed to a significant extent from below. This anticyclonic vortex will strengthen and eventually dominate at high levels. In terms of Fourier components, a quasi-stationary wave 1 amplifies on this date, in conjunction with the displacement of the cyclonic vortex from the polar position. These subplots confirm the intricate Lagrangian structures in the troposphere. The 18th of

Nonlin. Processes Geophys. Discuss., doi:10.5194/npg-2017-8, 2017
Manuscript under review for journal Nonlin. Processes Geophys.
Discussion started: 16 February 2017

Nonlinear Processes in Geophysics
Discussions
Open Access
EGU

October no yellow coherent features are visible in the upper stratosphere. The lowest of the horizontal sections, taken within the troposphere, confirms its chaotic nature.

We next address how M captures the invariant character of singular features found in the representations of M. Figure 5 a) shows a blue dark line near the edge of the polar vortex, around $45°$E. This feature is related to an invariant manifold that acts as a vertical barrier, which is several kilometers deep. This manifold structure is separating the two counterrotating vortex tubes just described. Further information on the singular features is given in Fig. 7. The black dots in Figs. 7a) and b) represents for 6th of October 1979, 00:00:00 UTC, the horizontal and vertical positions of a particle located on the feature indicated by the blue dark line in Fig. 5 a) at a height of 31.3km, longitude $90°$E and latitude $77.74°$S. The black dots in Figs. 7c) and d) show the corresponding locations of the same particle six hours later. The invariant character of the singular structure is confirmed as the particle remains on it during its evolution.

Similarly, let us consider a particle located at the hyperbolic point appearing in Fig. 6 a) at $z = 31.3$km at around $12°$E. Figure 8 shows the M function for a sequence of 2D slices obtained each at constant longitude. From one panel to the next, longitude changes tracking the particle motion. Again the invariant nature of the singular structures is confirmed while the particle evolves. Between frames a) to c) the particle approaches a hyperbolic point along the stable manifold, which is visible in the different slices. From frame d) onwards the particle moves away from the point along the unstable manifold. During this sequence of events the particle itself remains at an almost constant altitude as the invariant structures evolve in time. The small change in height is consistent with the quasi-isentropic flow on quasi-horizontal surfaces.

5 Conclusions

In the present paper we have introduced an algorithm for the visualization, analysis and validation of transport and mixing processes in three-dimensional atmospheric flows. The algorithm is based on the methodology of Lagrangian descriptors (LDs), a technique from Dynamical Systems Theory. Specifically, we have implemented the application of the full power of the function M computed with 3D trajectories, which hitherto had been used in 2D settings. The consistency of our development was verified by showing the similarity of results obtained from the full 3D scenario at a constant height with those obtained from the 2D scenario for a potential temperature surface that is at approximately the same height.

To demonstrate the methodology we have applied it to a numerical dataset describing the flow above Antarctica during the southern late winter and spring, with an emphasis on the final stratospheric warming of 1979. The dataset was obtained from ERA-Interim Reanalysis data provided by the ECMWF. The “final stratospheric warming” is characterized by the breakdown of the westerly SPV during the transition from winter to summer circulation. Our results confirm that the onset of this process is characterized by an initial decay of the vortex in the upper stratosphere where the circulation weakens, albeit it remains strong at lower heights. We have also captured the anticyclonic circulation that develops during October preferentially above the southern part of Australia.

A preliminary analysis of the 3D features provided by the methodology has provided insights that will be explored in future studies. The cyclonic westerly vortex during late winter appears to extend down to the troposphere. We have also found features

related to invariant manifolds that can act as a vertical barriers to transport between vortices. The particular feature found is several kilometers deep and we demonstrated that fluid parcels remain in this feature during intervals in the order of days. Such features may be important for the transport of chemical tracers in the stratosphere.

Acknowledgements. J. Curbelo, V. J. García-Garrido and A. M. Mancho are supported by MINECO grant MTM2014-56392-R. C. Niang acknowledges Fundacion Mujeres por Africa and ICMAT Severo Ochoa project SEV-2011-0087 for financial support. A. M. Mancho and C. Niang are supported by CSIC grant COOPB20265. The research of S. Wiggins is supported by ONR grant No. N00014-01-1-0769. C. R. Mechoso was supported by the U.S. NSF grant AGS-1245069. We also acknowledge support from ONR grant No. N00014-16-1-2492.

Nonlin. Processes Geophys. Discuss., doi:10.5194/npg-2017-8, 2017
Manuscript under review for journal Nonlin. Processes Geophys.
Discussion started: 16 February 2017

Nonlinear Processes in Geophysics
Discussions
Open Access
EGU

References

Aref, H. (1984). Stirring by chaotic advection. *J. Fluid Mech.*, **143**, 1–21.

Bettencourt, J. H., López, C., Hernández-García, E., Montes, I., Sudre, J., Dewitte, B., Paulmier, A., and Garçon, V. (2014). Boundaries of the peruvian oxygen minimum zone shaped by coherent mesoscale dynamics. *Nature Geoscience*, **8**, 937–940.

Bowman, K. P. (1993). Large-scale isentropic mixing properties of the Antarctic polar vortex from analyzed winds. *Journal of Geophysical Research*, **98**, 23013–23027.

Branicki, M. and Kirwan Jr., A. D. (2010). Stirring: The Eckart paradigm revisited. *Int. J. Eng. Sci.*, **48**, 1027–1042.

Branicki, M. and Wiggins, S. (2009). An adaptive method for computing invariant manifolds in non-autonomous, three-dimensional dynamical systems. *Physica D*, **238**(16), 1625 – 1657.

Branicki, M., Mancho, A. M., and Wiggins, S. (2011). A Lagrangian description of transport associated with a front-eddy interaction: application to data from the North-Western Mediterranean sea. *Physica D*, **240**(3), 282–304.

Cartwright, J. H. E., Feingold, M., and Piro, O. (1996). Chaotic adection in three-dimensional unsteady incompressible laminar flow. *J. Fluid Mech.*, **316**, 259–284.

de la Cámara, A., Mancho, A. M., Ide, K., Serrano, E., and Mechoso, C. (2012). Routes of transport across the Antarctic polar vortex in the southern spring. *J. Atmos. Sci.*, **69**(2), 753–767.

de la Cámara, A., Mechoso, R., Mancho, A. M., Serrano, E., and Ide., K. (2013). Isentropic transport within the Antarctic polar night vortex: Rossby wave breaking evidence and Lagrangian structures. *J. Atmos. Sci.*, **70**, 2982–3001.

Dee, D. P. *et al.* (2011). The ERA-Interim reanalysis: configuration and performance of the data assimilation system. *Quarterly Journal of the Royal Meteorological Society*, **137**(656), 553–597.

d'Ovidio, F., Isern-Fontanet, J., López, C., Hernández-García, E., and García-Ladona, E. (2009). Comparison between Eulerian diagnostics and finite-size Lyapunov exponents computed from altimetry in the Algerian basin. *Deep Sea Res. I*, **56**(1), 15–31.

du Toit, P. C. and Marsden, J. E. (2010). Horseshoes in hurricanes. *J. Fixed Point Theory Appl.*, **7**, 351–384.

Garcia-Garrido, V. J., Mancho, A. M., and Wiggins, S. (2015). A dynamical systems approach to the surface search for debris associated with the disappearance of flight MH370. *Nonlin. Proc. Geophys.*, **22**, 701–712.

Garcia-Garrido, V. J., Ramos, A., Mancho, A. M., Coca, J., and Wiggins, S. (2016). A dynamical systems perspective for a real-time response to a marine oil spill. *Marine Pollution Bulletin.*, pages 1–10.

García-Garrido, V. J., Curbelo, J., Mechoso, C. R., Mancho, A. M., and Wiggins, S. (2017). A simple kinematic model for the lagrangian description of relevant nonlinear processes in the stratospheric polar vortex. *Nonlin. Proc. Geophys. Discussion.*

Guha, A., Mechoso, C. R., Konor, C. S., and Heikes, R. P. (2016). Modeling rossby wave breaking in the southern spring stratosphere. *J. Atmos. Sci.*, **73**(1), 393–406.

Haller, G. and Yuan, G. (2000). Lagrangian coherent structures and mixing in two-dimensional turbulence. *Physica D*, **147**, 352–370.

Koh, T.-Y. and Legras, B. (2002). Hyperbolic lines and the stratospheric polar vortex. *Chaos*, **12**, 382–394.

Lekien, F. and Ross, S. D. (2010). The computation of finite-time lyapunov exponents on unstructured meshes and for non-euclidean manifolds. *Chaos*, **20**, 017505.

Lopesino, C., Balibrea-Iniesta, F., García-Garrido, V. J., Wiggins, S., and Mancho, A. M. (2017). A theoretical framework for lagrangian descriptors. to appear. *International Journal of Bifurcation and Chaos.*

Madrid, J. A. J. and Mancho, A. M. (2009). Distinguished trajectories in time dependent vector fields. *Chaos*, **19**, 013111.

Mancho, A. M., Hernández-García, E., Small, D., Wiggins, S., and Fernández, V. (2006). Lagrangian transport through an ocean front in the North-Western Mediterranean Sea. *J. Phys. Oceanogr.*, **38**(6), 1222–1237.

Mancho, A. M., Wiggins, S., Curbelo, J., and Mendoza, C. (2013). Lagrangian descriptors: A method for revealing phase space structures of general time dependent dynamical systems. *Communications in Nonlinear Science and Numerical Simulations*, **18**(12), 3530–3557.

Manney, G. L. and Lawrence, Z. D. (2016). The major stratospheric final warming in 2016: Dispersal of vortex air and termination of Arctic chemical ozone loss. *Atmospheric Chemistry and Physics Discussions*, **2016**, 1–40.

Mechoso, C. R. and Hartmann, D. L. (1982). An observational study of traveling planetary waves in the southern hemisphere. *Journal of the Atmospheric Sciences*, **39**(9), 1921–1935.

Mechoso, C. R., O'Neill, A., Pope, V. D., and Farrara, J. D. (1988). A study of the stratospheric final warming of 1982 in the Southern Hemisphere. *Quart. J. R. Meteor. Soc.*, **114**, 1365–1384.

Mendoza, C. and Mancho, A. M. (2010). The hidden geometry of ocean flows. *Phys. Rev. Lett.*, **105**(3), 038501.

Mendoza, C., Mancho, A. M., and Wiggins, S. (2014). Lagrangian descriptors and the assesment of the predictive capacity of oceanic data sets. *Nonlin. Proc. Geophys.*, **21**, 677–689.

Moharana, N. R., Speetjens, M. F. M., Trieling, R. R., and Clercx, H. J. H. (2013). Three-dimensional lagrangian transport phenomena in unsteady laminar flows driven by a rotating sphere. *Phys. Fluids*, **25**, 093602.

Pouransari, Z., Speetjens, M. F. M., and Clercx, H. J. H. (2010). Formation of coherent structures by fluid inertia in three-dimensional laminar flows. *J. Fluid Mech.*, **654**, 5–34.

Press, W. H., Teukolsky, S. A., Vetterling, W. T., and Flannery, B. P. (1992). *Numerical Recipes in C: The Art of Scientific Computing*. Cambridge University Press, New York, NY, USA.

Rabier, F. *et al.* (2010). The concordiasi project in antarctica. *Bulletin of the American Meteorological Society*, **91**(1), 69–86.

Rempel, E. L., Chian, A. C.-L., Brandenburg, A., Munuz, P. R., and Shadden, S. C. (2013). Coherent structures and the saturation of a nonlinear dynamo. *Journal of Fluid Mechanics*, **729**, 309–329.

Rutherford, B. and Dangelmayr, G. (2010). A three-dimensional lagrangain hurricane eyewall computation. *Quarterly Journal of the Royal Meteorological Society*, **136**, 1931–1944.

Rutherford, B., Dangelmayr, G., and Montgomery, M. T. (2012). Lagrangian coherent structures in tropical cyclone intensification. *Atmospheric Chemistry and Physics*, **12**, 5483–5507.

Rypina, I. I., Pratt, L. J., Wang, P., Özgökmen, T. M., and Mezic, I. (2015). Resonanace phenomena in a time-dependent, three-dimensional model of an idealized eddy. *Chaos*, **25**, 087401.

Shadden, S. C., Lekien, F., and Marsden, J. E. (2005). Definition and properties of Lagrangian Coherent Structures from finite-time Lyapunov exponents in two-dimensional aperiodic flows. *Physica D*, **212**, 271–304.

Simmons, A., Uppala, S., Dee, D., and S, K. (2007). ERA-Interim: New ECMWF reanalysis products from 1989 onwards. *ECMWF Newsletter*, **110**, 25–35.

Smith, M. L. and McDonald, A. J. (2014). A quantitative measure of polar vortex strength using the function m. *J. Gephys.Res. Atmos.*, **119**, 5966–5985.

Wiggins, S. (2010). Coherent structures and chaotic advection in three dimensions. *J. Fluid Mech.*, **654**, 1–4.

Yamazaki, K. and Mechoso, C. R. (1985). Observations of the final warming in the stratosphere of the southern hemisphere during 1979. *J. Atmos. Sci.*, **42**, 1198–1205.

Nonlin. Processes Geophys. Discuss., doi:10.5194/npg-2017-8, 2017
Manuscript under review for journal Nonlin. Processes Geophys.
Discussion started: 16 February 2017

Nonlinear Processes in Geophysics
Discussions
Open Access
EGU

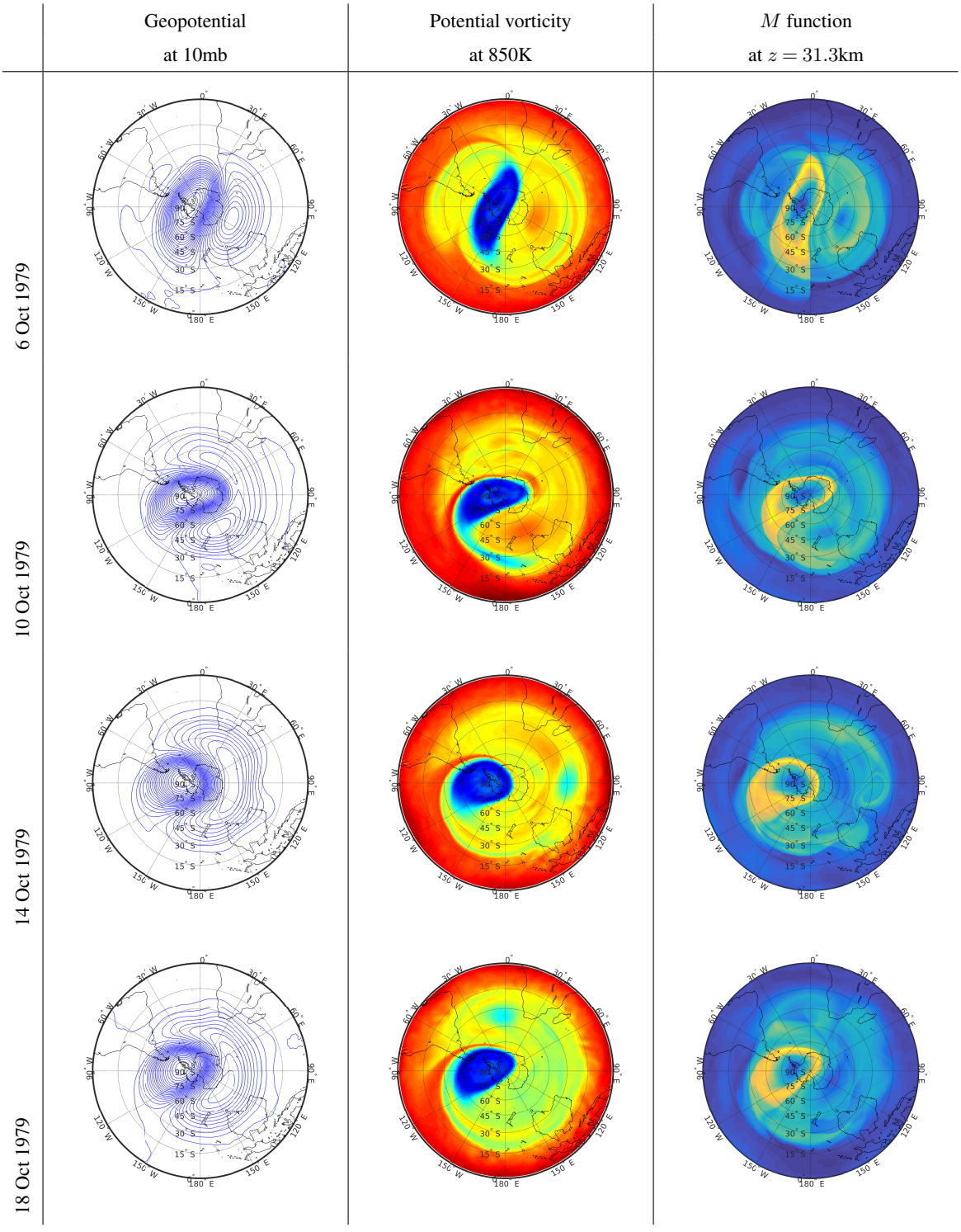

Figure 2. Comparison of Geopotential at constant Pressure 10mb, Potential Vorticity at 850K and M function at $z = 31.3$km for several days of October 1979

Nonlin. Processes Geophys. Discuss., doi:10.5194/npg-2017-8, 2017
Manuscript under review for journal Nonlin. Processes Geophys.
Discussion started: 16 February 2017

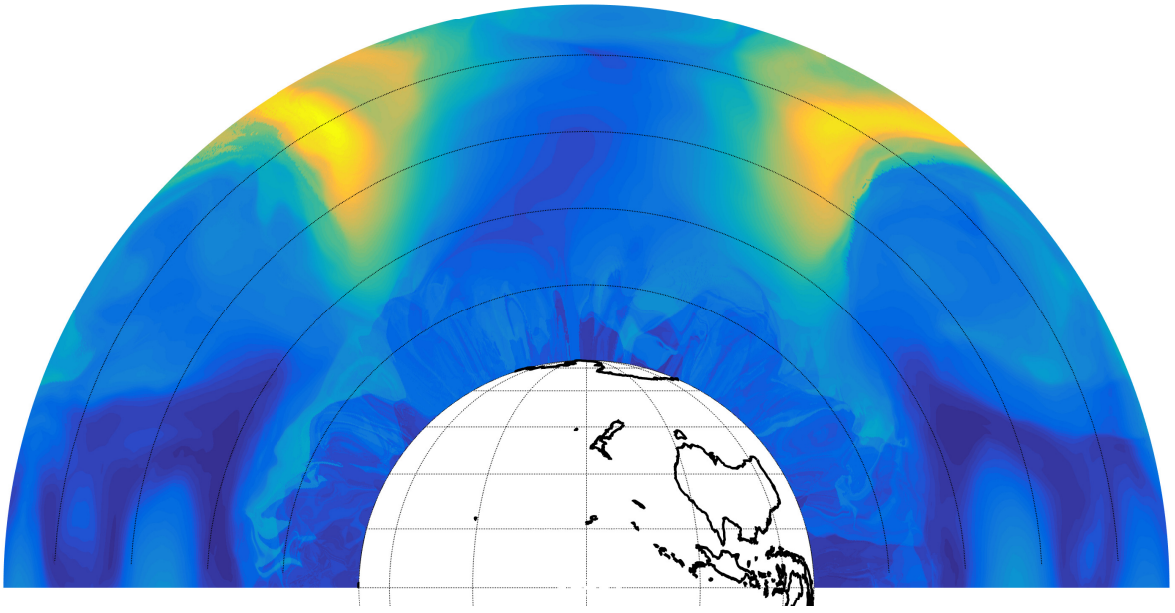

Figure 3. 15 August 1979 00:00:00 UTC. M for $\tau = 5$ days displayed along the vertical slice passing through longitudes 90^{o}W and 90^{o}E. The black lines correspond to height 10, 20, 30 and 40km.

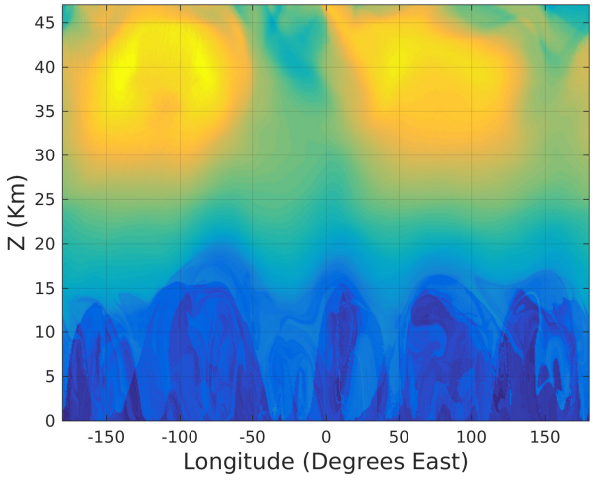

Figure 4. 15 August 1979 00:00:00 UTC. M for $\tau = 5$ days displayed along the vertical slice passing through latitude 60°S.

Nonlin. Processes Geophys. Discuss., doi:10.5194/npg-2017-8, 2017
Manuscript under review for journal Nonlin. Processes Geophys.
Discussion started: 16 February 2017

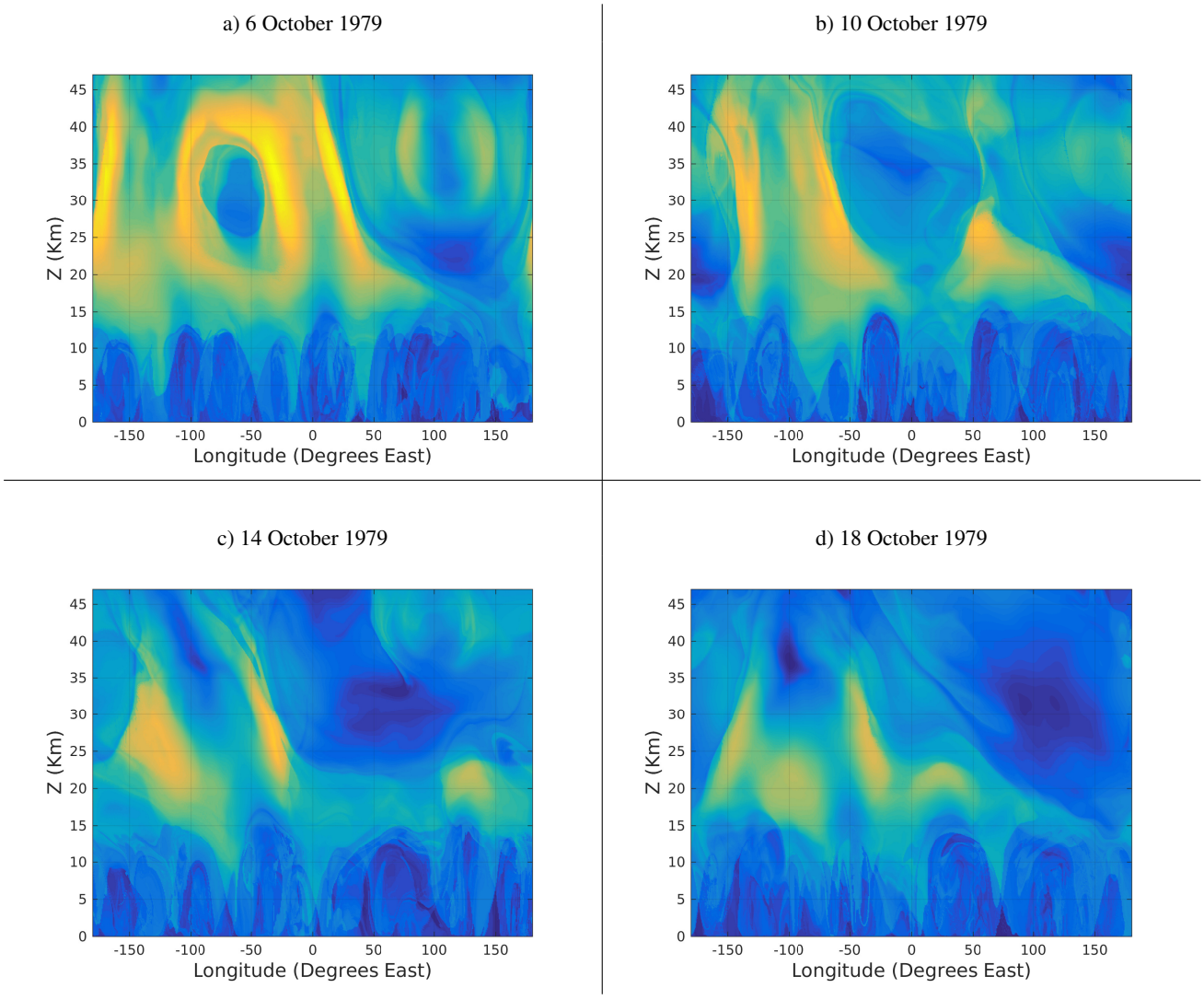

Figure 5. Vertical slices showing M for $\tau = 5$ at constant latitude 60°S at four selected days in October. The color scale is the same in all figures.

Nonlin. Processes Geophys. Discuss., doi:10.5194/npg-2017-8, 2017
Manuscript under review for journal Nonlin. Processes Geophys.
Discussion started: 16 February 2017

Nonlinear Processes in Geophysics
Discussions
Open Access
EGU

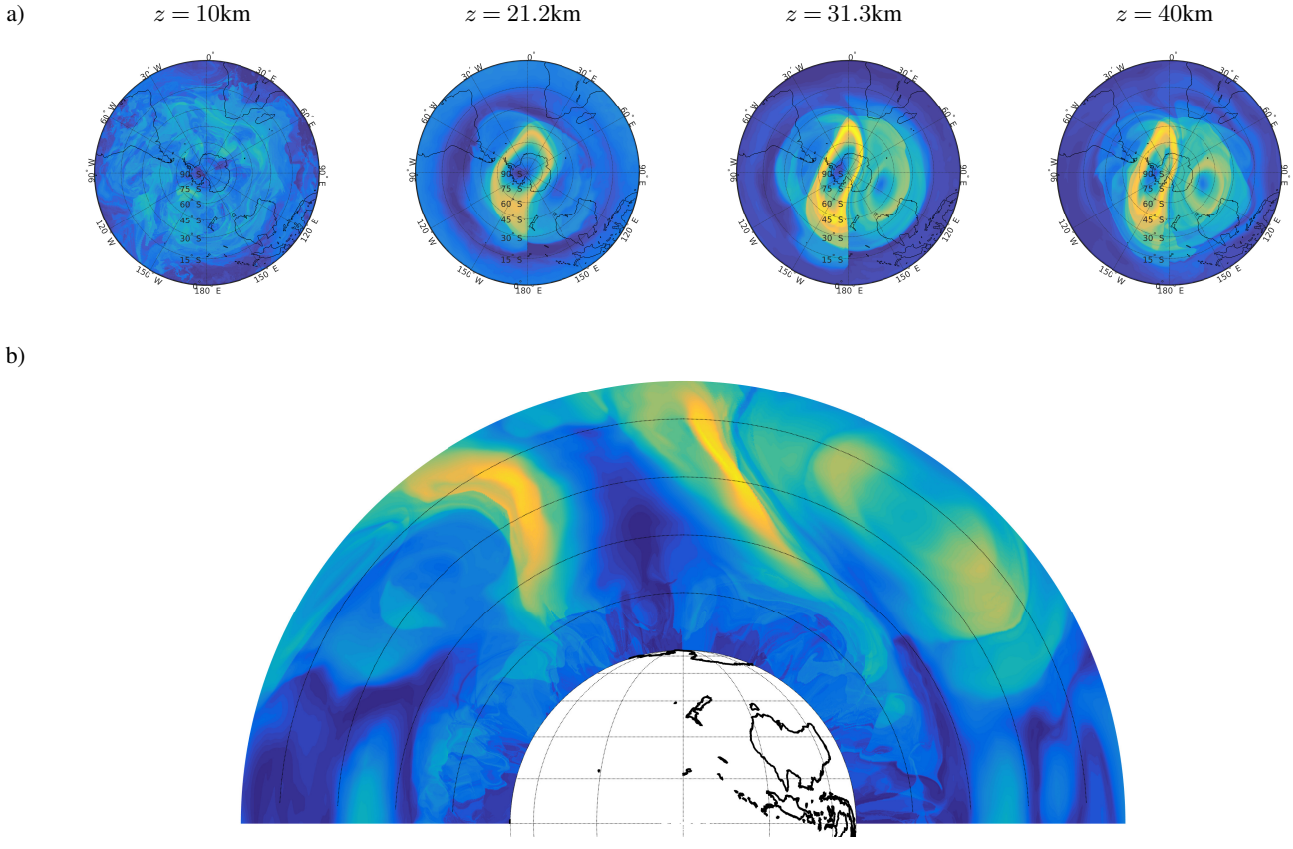

Figure 6. 6 October 1979 00:00:00 UTC. a) Slices of M at constant heights $z = 10, 21.2, 31.3$ and 40km with $\tau = 5$; b) Slice of M at constant longitude $\lambda = 90^\circ W$ and $\lambda = 90^\circ E$). The black lines in b) correspond to 10, 20, 30 and 40km.

Nonlin. Processes Geophys. Discuss., doi:10.5194/npg-2017-8, 2017
Manuscript under review for journal Nonlin. Processes Geophys.
Discussion started: 16 February 2017

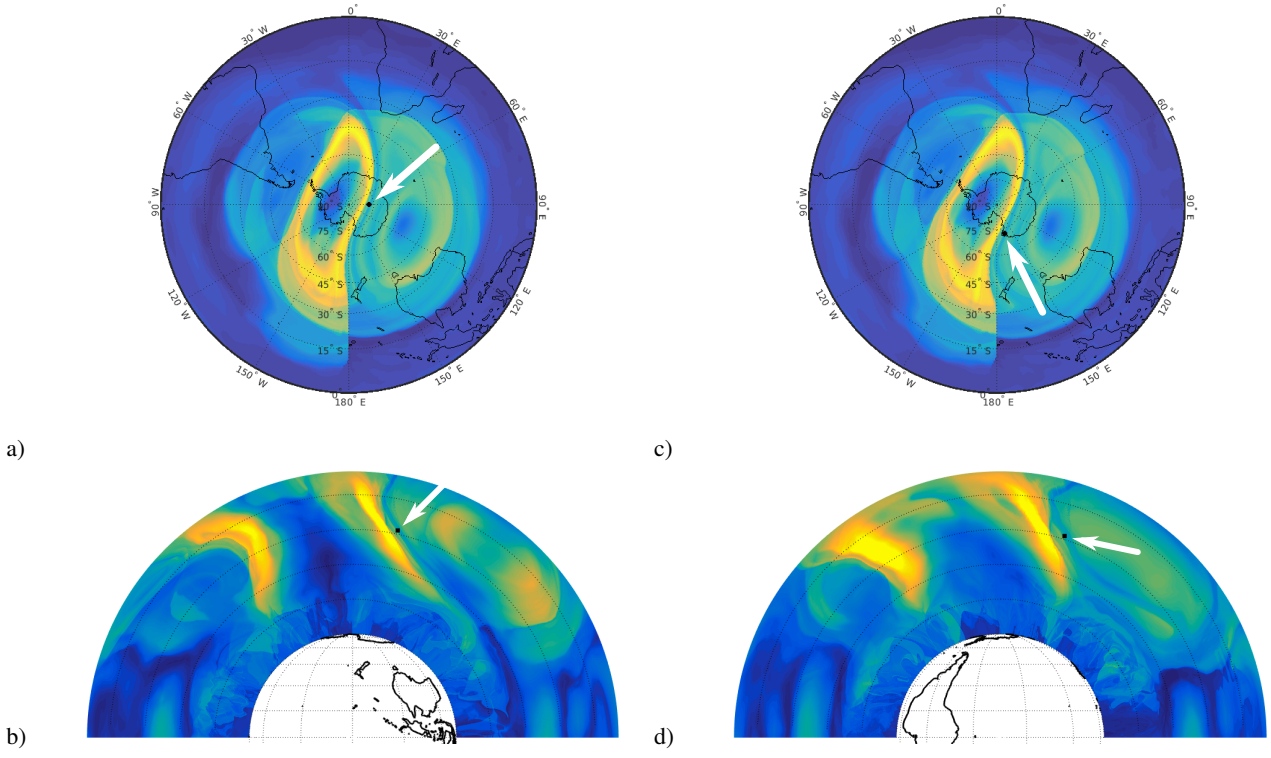

Figure 7. Evaluation of the M function with a black particle on it. a) The black particle is placed exactly over an invariant manifold on a 2D slice obtained at height of 31.3 km on the 6 of October 1979 00:00:00 UTC; b) the same black particle on the same day and time placed on a 2D slice obtained at longitude $90^o E$; c) the same black particle six hours later on a 2D slice of M obtained at the corresponding height of the particle at that time; d) the same black particle six hours later on a 2D slice of M obtained at the corresponding longitude of the particle at that time.

Nonlin. Processes Geophys. Discuss., doi:10.5194/npg-2017-8, 2017
Manuscript under review for journal Nonlin. Processes Geophys.
Discussion started: 16 February 2017

Nonlinear Processes in Geophysics
Discussions
Open Access
EGU

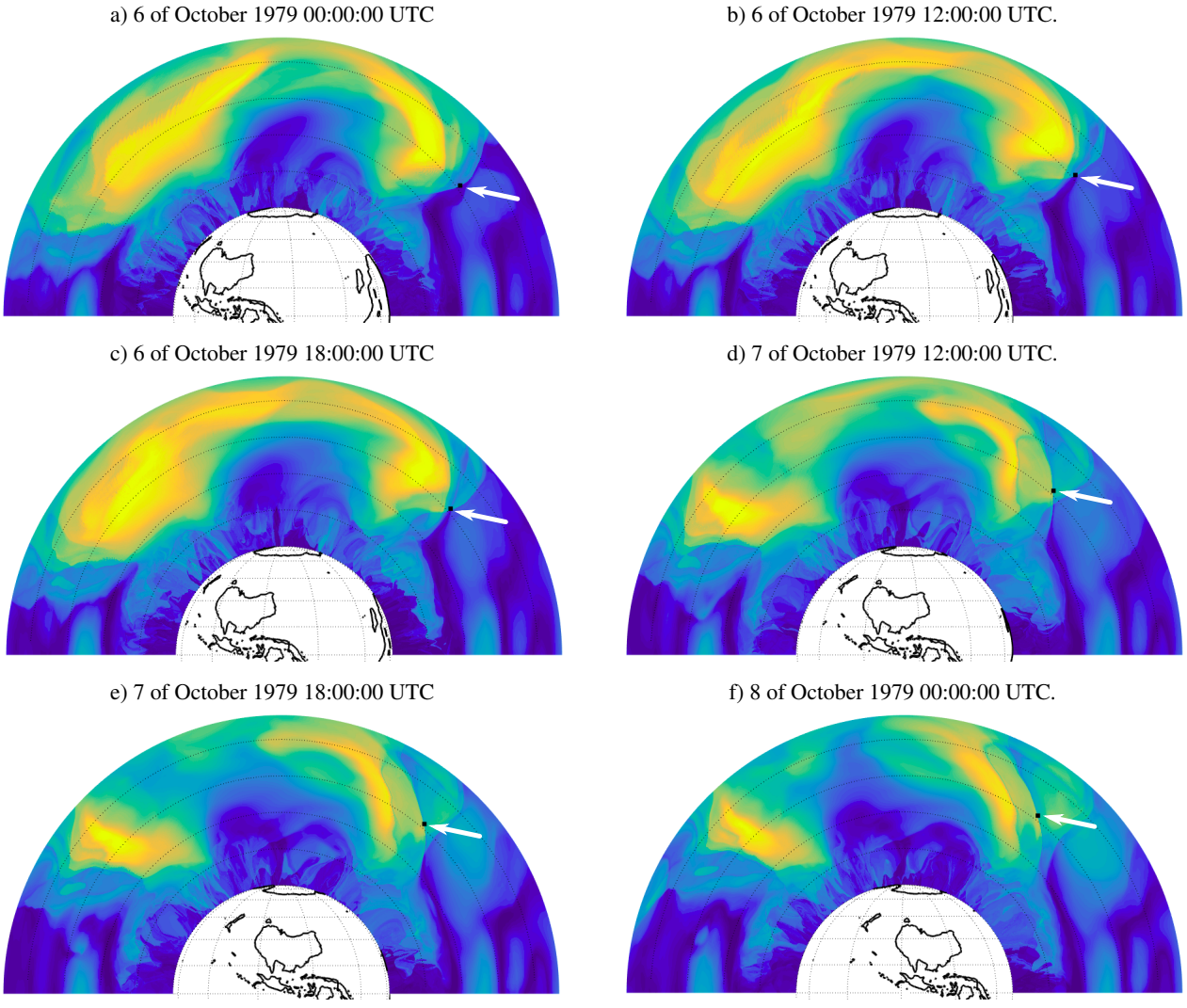

Figure 8. Evaluation of the M function with a black particle at different longitudes. a) The black particle is placed on an invariant manifold on a 2D slice obtained at constant longitude 12^oW on the 6 of October 1979 00:00:00 UTC; b) the same black particle on a plane with constant longitude on the 6 of October 1979 12:00:00 UTC; c) the black particle on a plane with constant longitude on the 6 of October 1979 18:00:00 UTC; d) the black particle on a plane with constant longitude on the 7 of October 1979 12:00:00 UTC; e) the black particle on a plane with constant longitude on the 7 of October 1979 18:00:00 UTC; f) the black particle on a plane with constant longitude on the 8 of October 1979 00:00:00 UTC.